Available online at www.sciencedirect.com
SCIENCE DIRECT®
Journal of Magnetic Resonance 169 (2004) 196–202
JMR Journal of Magnetic Resonance
www.elsevier.com/locate/jmr

Feasibility of diffusion-NMR surface-to-volume measurements tested by calculations and computer simulations

Mark S. Conradi,[a,b,*] Matthew A. Bruns,[a] Alexander L. Sukstanskii,[b] Samuel S. Gross,[a] and Jason C. Leawoods[a]

[a] Department of Physics, Washington University, St. Louis, MO 63130-4899, USA
[b] Department of Radiology, Washington University, St. Louis, MO 63130-4899, USA

Received 29 December 2003; revised 14 April 2004
Available online 18 May 2004

Abstract

It has been demonstrated previously that the surface-to-volume ratio S/V can be determined from the derivative of the time-dependent diffusion coefficient $D_{(t)}$, in the limit $t \to 0$. Several questions arise concerning the practicality of determining S/V by NMR. In particular, how large are the errors generated by (1) working outside the $t \to 0$ limit and (2) measuring D outside the $b \to 0$ limit, both for narrow and full-width gradient pulses? Here b is $\gamma^2 G^2 \delta^2 \Delta$ for narrow pulses and $\gamma^2 G^2 t^3/12$ for broad pulses. These questions are addressed by random-walk computer simulations and numerical calculations in geometries relevant to small-airways of lung. The results demonstrate that one can work well outside the $t \to 0$ and $b \to 0$ limits, provided 10–20% accuracy in the measured S/V is sufficient. Emphasis is placed on the useful range of times t for which NMR determinations of lung S/V are feasible.

1. Introduction

The time dependence of the diffusivity $D_{(t)}$ contains much information [1,2] about the restrictions to diffusive motions. In particular Mitra, Sen, and Schwartz (MSS) showed that at short times t

$$\frac{D_{(t)}}{D_0} = 1 - \left[\frac{4}{3d\sqrt{\pi}}\right]\frac{S}{V}\sqrt{D_0 t}, \tag{1}$$

where d is the dimensionality, D_0 is the unrestricted diffusion coefficient, and S/V is the surface-to-volume ratio [3,4]. The MSS formula is the first two terms in a Taylor series for $D_{(t)}$ in powers of $\sqrt{t}$; there are higher-power terms important at longer times, including corrections for curvature and corners of the surface [3,5,6]. Strictly, the term involving S/V is essentially the derivative of $D_{(t)}$ with respect to $\sqrt{t}$, in the limit of zero time t. A simple physical picture [5] of the S/V term is based on the volume fraction of spins within "striking distance" $\sqrt{D_0 t}$ of the walls. The MSS equation refers to an isotropic situation with $D_{(t)}$ defined by mean-squared displacement: $D_{(t)} = \overline{(\Delta r)^2}/2dt$. This is equivalent to the diffusivity measured by pulsed-field gradients (PFG) in the narrow-pulse (NP) limit for $b \to 0$ (b has the usual meaning and is conjugate to D; for narrow gradient pulses of amplitude G, width δ, and separation Δ, b is $\gamma^2 G^2 \delta^2 \Delta$, with $\delta \ll \Delta$). We note that working in the small b limit guarantees that the signal attenuation is small, so all spins are weighted equally and the true average diffusivity is obtained.

The case of static (dc)-field gradients with a π-pulse for refocusing is equivalent to the experiment where full-width gradient pulses are used, turning off only long enough for the RF pulses and spin-echo acquisition. This wide-pulse or spin-echo (SE) case has been treated [6]; in the short-time limit, an equation analogous to (1) results:

$$\frac{D_{(t)}}{D_0} = 1 - \left[\frac{32}{\sqrt{\pi}d35}\left(\frac{2\sqrt{2}-1}{\sqrt{2}}\right)\right]\frac{S}{V}\sqrt{D_0 t}. \tag{2}$$

Here the time t is twice the spacing τ between the RF pulses envisioned in [6]. Again, this formula is an aver-

* Corresponding author. Fax: 1-314-935-6219.
E-mail address: msc@wuphys.wustl.edu (M.S. Conradi).

1090-7807/$ - see front matter © 2004 Elsevier Inc. All rights reserved.
doi:10.1016/j.jmr.2004.04.014

age diffusivity, so it applies in the small b limit (for static field gradients or full-width gradient pulses, b is $\gamma^2G^2t^3/12$). The coefficient in square brackets in Eq. (2) is slightly smaller than that in (1), by a factor of 0.8866. This decrease is expected, because the *mean* diffusion time in the wide pulse case is somewhat smaller than t.

NMR methods are routinely used [7–10] to measure $D_{(t)}$, so it seems that NMR determinations of S/V should be straightforward using the results (1) and (2). We assume the free diffusivity D_0 is known by measurements on the same gas or gas mixture in bulk, outside the restricting structure. Eqs. (1) and (2) can be inverted to yield S/V from diffusion measurements in the narrow-pulse and spin-echo cases:

$$\left(\frac{S}{V}\right)_{\mathrm{NP}} = \left(1-\frac{D^{\mathrm{NP}}_{(t)}}{D_0}\right)\frac{3d\sqrt{\pi}}{4}(D_0t)^{-1/2}, \tag{3a}$$

$$\left(\frac{S}{V}\right)_{\mathrm{SE}} = \left(1-\frac{D^{\mathrm{SE}}_{(t)}}{D_0}\right)\frac{35d\sqrt{\pi}}{32}\left(\frac{\sqrt{2}}{2\sqrt{2}-1}\right)(D_0t)^{-1/2}. \tag{3b}$$

However, two important issues need to be addressed.

1. Experimentally, it is impossible to evaluate Eqs. (3a) and (3b) in the limit of zero time. Fundamentally, this involves measuring the difference between nearly equal quantities, $D_{(t)}$ and D_0, which is notoriously difficult in the face of measurement noise. In addition, working at small t requires very intense gradients with (at least in the narrow-pulse case) very small rise and fall times, eventually outstripping the capabilities of any hardware. Thus, we ask how large can t become (or how far can $D_{(t)}/D_0$ fall below one) for formulas (3a) and (3b) to remain valid, to within an allowable range of error?
2. In a system with restricted diffusion, a distribution of D values is present, with smaller D characterizing spins near the restricting walls. Thus, one neither expects nor obtains [11,12] single-exponential decays of signal amplitude versus b value. One can obtain the average diffusivity, equally weighted across all spins, by using

$$D \equiv \frac{-1}{b}\ln(\mathcal{S}/\mathcal{S}_0), \tag{4}$$

in the limit of zero b, where $\mathcal{S}$ is the b-dependent attenuated signal amplitude and $\mathcal{S}_0$ is the $b=0$, unattenuated amplitude. Of course, working at small b involves taking the difference of nearly equal quantities, $\mathcal{S}$ and $\mathcal{S}_0$, which is unreliable with real (noisy) data. So we ask how much error is generated by determining D in a more practical way, such as $D \equiv 1/b^*$, where b^* is the value of b for which the signal amplitude $\mathcal{S}(b^*)$ is $1/e$ of $\mathcal{S}_0$?

Working with narrow gradient pulses is impractical in the short time limit, $t \to 0$. Narrow pulses require extremely large gradient amplitudes, for a given b value. Because of the gradient coil inductance, excessively large voltages are required to switch the gradient. Corrections for finite pulse widths have been reported [13]. Thus, the wide pulse case [14,15] is more relevant to experiment, in general. This includes the technically less-demanding case of static gradients [16,17] used with a π-refocusing RF pulse (spin echo, SE).

We investigate here the importance of these practical issues in applying the results (1) and (2) to NMR determinations of S/V. In addition to numerical calculations, restricted gas diffusion is simulated by computer-generated random walks. We focus on geometries that are relevant to the small-airways of lungs, in which 95% or more of the gas resides [18,19]. NMR/MRI measurements have shown the diffusion of ^{3}He gas in lungs to be substantially restricted in healthy lungs. Airway expansion and tissue destruction in the disease emphysema [20] result in large increases in the measured diffusivity [21–23]. An MRI measurement of surface-to-volume S/V on a pixel-by-pixel basis would be very valuable for understanding the changes in emphysematous lungs, both in general and for specific patients. At present, the only in vivo lung S/V measurements are global (entire lung) and are taken from the rate of CO uptake (so-called diffusing capacity) [18,20].

2. Methods

Computer simulations of random-walks were performed on N independent particles, with N typically 10^4–10^5, in the cylindrical geometry displayed in Fig. 1. As introduced elsewhere [23], this is a reasonably accurate and easily implemented representation of a typical small-airway lined with alveoli. In particular, the use of infinitely long, straight cylinders is a good approximation for the short diffusion times relevant to determinations of surface-to-volume S/V. Each particle was assigned a random starting position and was allowed to move at intervals of time Δt; Δt was 0.01 μs in most of the simulations. At each step, the particle was moved with equal probability in one of six directions $(\pm x, \pm y, \pm z)$. The step length was fixed at $\sqrt{6D_0\Delta t}$ with

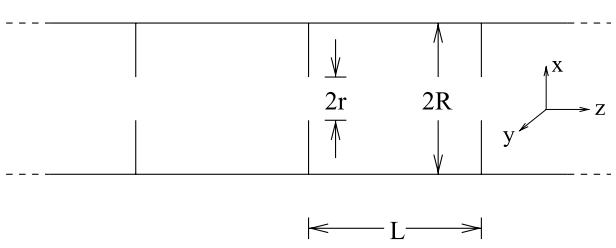

Fig. 1. Cylindrical geometry used for simulations of diffusion. The cylinder axis runs left–right. Each section of length L is separated from neighboring sections by partially open, washer-like partitions.

$D_0 = 0.88\,\mathrm{cm}^2/\mathrm{s} = 88\,\mu\mathrm{m}^2/\mu\mathrm{s}$, which describes ^{3}He gas dilute in air or N_2 (thus a step length of 2.3 μm). If the selected move would carry the particle through any wall, the move was rejected and the particle remained at the initial position. This style of simulation is crude *for each step*: fixed jump distance, only six step directions, and no attempt to have the particles properly reflect from the walls. The very short-time step Δt (and the correspondingly large number of steps in a given simulated time) make these issues insignificant. In our view, a short Δt with a simple jump-algorithm, as used here, is the preferred method.

While the simulations were performed for cylinders of specific sizes with a gas of specific free diffusivity D_0, the presented results can be scaled to yield results for other D_0 values and cylinder sizes. Consider the transverse diffusivity [23], which depends only on R, D_0, and time t (specifically independent of r and L; see Fig. 1). Two systems A and B are said to be in correspondence (as in thermodynamic corresponding states [24]) if

$$\frac{D_{0,A}t_A}{R_A^2} = \frac{D_{0,B}t_B}{R_B^2}, \tag{5}$$

because $D_0 t/R^2$ is the *only* dimensionless parameter [25] characterizing the problem. Thus, the time-dependent transverse diffusivities of A and B are related by the dimensionless ratios

$$\frac{D_{A(t_A)}}{D_{0,A}} = \frac{D_{B(t_B)}}{D_{0,B}}, \tag{6}$$

provided the times t_A and t_B are related as in Eq. (5). Similar scaling applies for the longitudinal diffusion (along the tube axis in Fig. 1), except that $D_{(t)}$ now depends on D_0, t, R, r, and L. So, systems are in correspondence provided they obey Eq. (5) and have similar shapes (i.e., the same ratios L/R and r/R).

The simulations were used to calculate mean-squared displacements in each of the directions x, y, and z. Time-dependent diffusivities were defined from the mean-squared displacements as

$$\begin{aligned} D_x^{\mathrm{NP}} &\equiv \overline{(\Delta x)^2}/2t \quad \text{and} \\ D_3^{\mathrm{NP}} &\equiv \left[\overline{(\Delta x)^2} + \overline{(\Delta y)^2} + \overline{(\Delta z)^2}\right]/6t, \end{aligned} \tag{7}$$

in 1-D and 3-D. The NP (narrow pulse) designation serves to remind that PFG experiments with narrow pulses in the $b \to 0$ limit yield the diffusivity values from mean-squared displacement, (7). In addition, normalized NMR signal amplitudes $\mathcal{S}$ were calculated in the wide-pulse or spin-echo (SE) case from the NMR spin-precessional phase shifts ψ, with $\mathcal{S} = \langle e^{i\psi}\rangle = \langle \cos\psi\rangle$, where the average is over the N particles in the simulation. In general, for a gradient along the x-axis,

$$\psi_{(t)} = \gamma \int_{t'=0}^{t} G_{(t')} X_{(t')}\, \mathrm{d}t', \tag{8}$$

where $G_{(t')}$ is the effective gradient (i.e., the actual gradient with sign inversion at the π pulse). We employ a static (constant) actual gradient, corresponding to a square wave effective gradient: G from time zero to $t/2$ and $-G$ from $t/2$ to t. The integral is re-written as a discrete sum

$$\psi_{(t)} = \gamma G(\Delta t)\left(\sum_{j=0}^{T/2} x_j - \sum_{j=T/2}^{T} x_j\right), \tag{9}$$

where Δt is the time step duration and j is the (integer) time-step-number, with $T \equiv t/\Delta t$. For this gradient waveform, the weighting parameter b is given [26] by $\gamma^2 G^2 (t/2)^3 2/3$. Thus, the phase ψ for any particle can be expressed in terms of its trajectory and b,

$$\psi_{(t)} = \sqrt{12b/t^3}(\Delta t)\left(\sum_{j=0}^{T/2} x_j - \sum_{j=T/2}^{T} x_j\right). \tag{10}$$

For weak b, resulting in small spin phases ψ, $\langle\cos\psi\rangle$ is $1 - \langle\psi^2\rangle/2$. Equating this to $e^{-bD_x} = 1 - bD_x$, we obtain the NMR-determined D_x^{SE} with constant gradients, taken in the $b \to 0$ limit,

$$D_x^{\mathrm{SE}} = \left[6(\Delta t)^2/t^3\right]\overline{\left[\sum_{j=0}^{T/2} x_j - \sum_{j=T/2}^{T} x_j\right]^2}, \tag{11}$$

where the overbar denotes averaging over all N particles. We note that the mathematics of the $b \to 0$ limit are the same as the Gaussian phase distribution approximation, for arbitrary b. Eq. (11) allows D^{SE} to be computed without explicitly considering the $b = 0$ limit.

The above discussion can readily be generalized to gradient directions other than x. For an assortment of randomly oriented objects, the three-dimensional powder average wide-pulse diffusivity D_3^{SE} can be computed in a form similar to Eq. (11) as

$$\begin{aligned} D_3^{\mathrm{SE}} = \left[6(\Delta t)^2/t^3\right]\Bigg\{&\overline{\left[\sum_{j=0}^{T/2} x_j - \sum_{j=T/2}^{T} x_j\right]^2} \\ &+ \overline{\left[\sum_{j=0}^{T/2} y_j - \sum_{j=T/2}^{T} y_j\right]^2} + \overline{\left[\sum_{j=0}^{T/2} z_j - \sum_{j=T/2}^{T} z_j\right]^2}\Bigg\}\Big/3. \end{aligned} \tag{12}$$

We note that many simulations of bounded diffusion have been reported [11,16,27], some specifically relevant to the MSS equation for surface-to-volume ratio [3,4,6]. Analytical approaches to restricted diffusion have been reported [23,28], although these assume the Gaussian phase approximation. The work here is focused upon addressing the issues enumerated at the end of the Introduction, to assess the feasibility of MRI measurements of local surface-to-volume ratio in lungs.

All determinations of initial positions and the directions of each step were performed with the random

number generator provided by the GSL (GNU Scientific Library), a numerical methods library for the C programming language.

3. Tests

The computer simulation algorithm was thoroughly tested to ensure its proper functioning. (i) For open tubes ($r = R$ in Fig. 1), the longitudinal diffusion D_z^{NP} in Eq. (7) was found to be very close to D_0. The typical error was about 1%. (ii) For closed tubes ($L = R = 150\,\mu\mathrm{m}$ and $r = 0$), the long-time asymptotic values of $\overline{(\Delta z)^2}$ and $\overline{(\Delta x)^2}$ were compared to the theoretical values of $L^2/6$ and $R^2/2$, respectively. Agreement to better than 1% was found. (iii) We explicitly tested the scaling formula (6), by comparing transverse diffusivities of the same gas in cylinders of $R = 150$ and $350\,\mu\mathrm{m}$. After scaling times in the larger cylinders by $(2.333)^2$, according to Eq. (5), the data were the same to within the numerical noise. (iv) Long-time longitudinal diffusivity in the structure of Fig. 1 is bounded by $D_{z(t)} \leqslant D_0$ because of the restrictions by the partitions, and $D_{z(t)} \geqslant D_0(r/R)^2$. This last bound uses the fraction of open area of the partitions; $D_{z(t)}$ would equal $D_0(r/R)^2$ in the case of $L \ll r$. The above inequalities were always obeyed in the long-time limit.

4. Results

Simulations have been performed on cylinders with the geometry presented in Fig. 1 for a wide range of parameters. Representative results appear in Fig. 2 for the cases of closed cells ($r = 0$), partly open cells ($r = 0.7R$), and fully open cells (smooth-wall tubes, $r = R$), from top to bottom. Diffusivities calculated from the random-walk mean-squared displacements during time t (D_3^{NP}) from Eq. (7) appear as solid curves. Open circles represent the diffusivity calculated from the NMR signal in the $b = 0$ limit, with a static-field gradient (spin echo or wide pulse, SE). All the diffusivities in Fig. 2 are three-dimensional orientational averages, using Eqs. (7) and (12). We note that the trends evident in the results of Fig. 2 are confirmed in the many other simulation results obtained but not shown here.

All of the diffusivities in Fig. 2 approach the free value of $D_0 = 88\,\mu\mathrm{m}^2/\mu\mathrm{s}$ at short times, as expected. In the case of D_3^{SE}, where the first point is at $t = 20\,\mu\mathrm{s}$, the D_0 value is never obtained. We note that the data should decrease as $\sqrt{t}$ at short times, resulting in an infinitely negative slope at zero time. At short times, D_3^{SE} decreases more slowly than does D_3^{NP}. This is to be expected, since the NMR measurement with static gradients (as opposed to the delta-spike gradients, NP) measures a displacement over a time interval somewhat

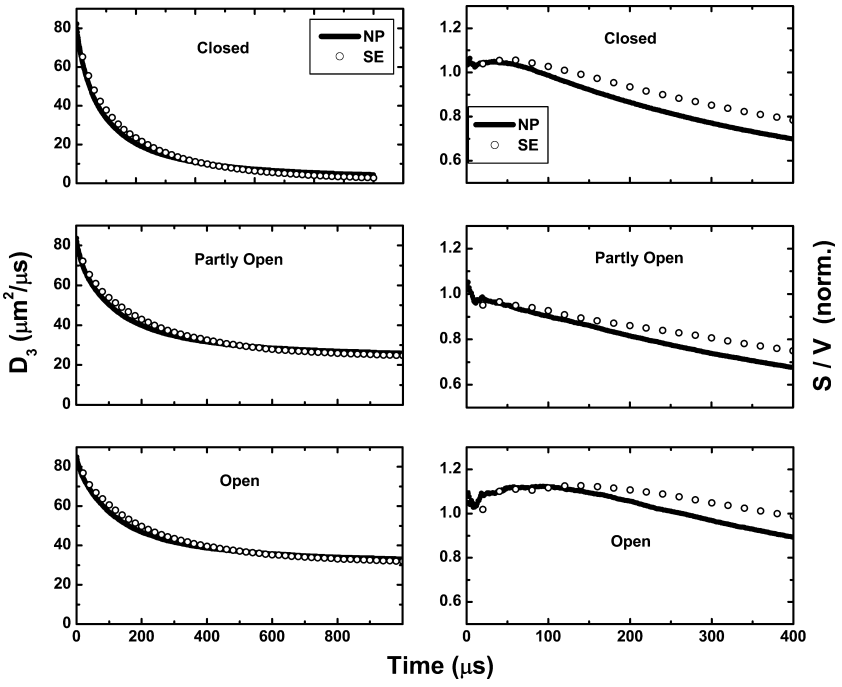

Fig. 2. Three-dimensional powder average diffusivities (at left) and surface-to-volume ratios S/V (at right) from Eqs. (3a) and (3b), as functions of the diffusion-measuring time. Results are shown for the cylindrical geometry of Fig. 1 with $R = 150\,\mu\mathrm{m}$ and $L = 150\,\mu\mathrm{m}$. From top to bottom, the cases treated are closed partitions ($r = 0$), partly open partitions ($r = 105\,\mu\mathrm{m}$, so the opening is 49% of the total area), and fully open (no partitions, $r = R$). The solid curves are from mean-squared displacement and correspond to the narrow pulse (NP) NMR PFG experiment; the open circles are from simulated NMR signal decays using a static gradient in the $b = 0$ limit (wide pulse or spin echo, SE). At right, the S/V is normalized by the actual S/V calculated from geometry.

smaller than t, as discussed below Eq. (2) . Hence, for a given decrease in $D_{(t)}$, the static gradient NMR experiment requires a somewhat larger time t. At long times, when most gas atoms have contacted the walls one or more times, D_3^{SE} becomes *smaller* than D_3^{NP}. This decrease is due to motional averaging [23,26] during each half of the NMR experiment (between the RF pulses and from the π-pulse to the echo). Such averaging *during* each gradient lobe clearly cannot occur with delta-spike gradient pulses (NP measurement). At very long times, one expects D_3 to be determined completely by longitudinal motion, because the transverse motion is fully restricted. The $t \to \infty$ limiting values of D_3 of the closed and open cases are thus expected to be 0 and $D_0/3$ (or $28.7\,\mu m^2/\mu s$), respectively. While $t = 1000\,\mu s$ is not quite long enough for these limits to attain, the data approach the above values.

The $D_{(t)}$ data from the left panels of Fig. 2 were used to calculate the surface-to-volume ratios S/V in the right panels, using Eqs. (3a) and (3b), for narrow and wide pulses, respectively. The S/V values are normalized by the actual S/V calculated from geometry. In all cases, the S/V values are *approximately* correct at short times and decrease at longer times. The decrease is, of course, due to $D_{3(t)}$ approaching an asymptotic value at long times, as discussed above.

In the case of the open smooth-wall tube, we confirmed that the increase in $(S/V)_{NP}$ above the actual geometric value of $2/R$ is explained by including the correction in the MSS formula (1) for surface curvature [3]. We note that all of the other cases have corners and sharp-edged holes on the interiors of the partitions, so that these cases require additional corrections [3]. We have not included such corrections, because they involve curvatures and corner-angles that are not known a priori to the measurer.

The S/V values derived from D_3^{NP} are within $\pm 15\%$ of the actual geometrical value for times $\leqslant 150\,\mu s$. Over the time window of 0–200 μs, the S/V taken from D_3^{SE} is within the $\pm 15\%$ range. We note that, in all three cases shown in Fig. 2, this time window can be expressed as including all values of D_3^{SE}/D_0 greater than 0.6. This is a surprisingly large region for the validity of a formula derived for the $t = 0$, "barely restricted" limit. Indeed, we note that the 200 μs window, for the system of closed cells, includes values of D_3^{SE}/D_0 as small as 0.25.

NMR signal amplitude decays for the static gradient spin echo (wide pulse, SE) are presented in Fig. 3. The time is held fixed as b is varied by varying the gradient strength. In each case, the straight solid line represents the slope of the initial decay, the $b = 0$ limit. Thus, the negative of this slope is the true average restricted diffusivity, equally weighting all the spins in the sample. The open circles are the simulated NMR spin-echo decays as functions of b. In some cases, the deviation from the simple exponential is positive while in others it is

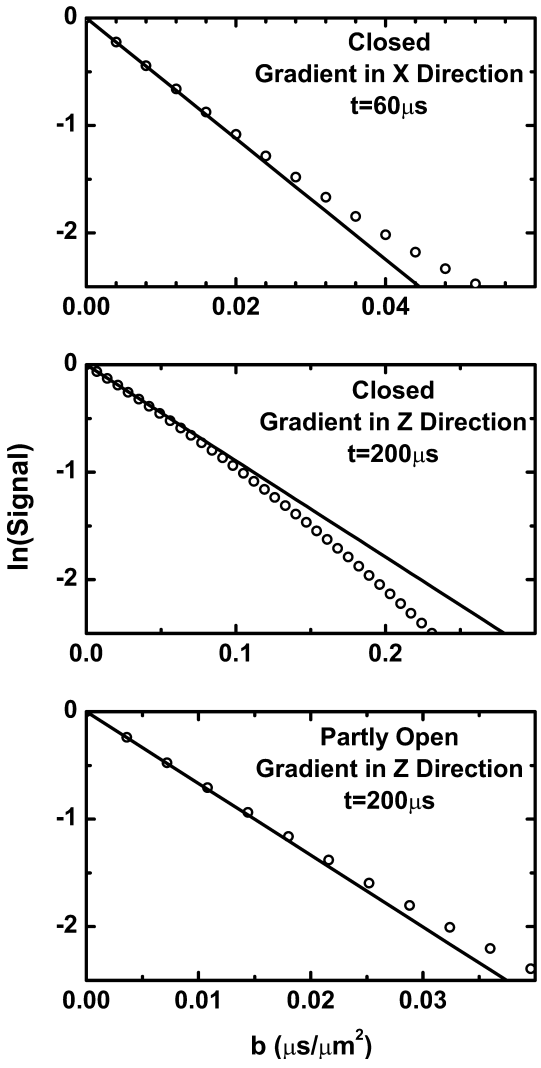

Fig. 3. NMR signal decays using full-width gradient pulses (SE case) from random-walk simulations. The straight solid lines represent the slope in the $b = 0$ limit; the negative of this slope is the average diffusivity, weighting all particles equally. The open circles are the natural logs of the normalized signal amplitudes S/S_0 as functions of b. Upper: diffusion transverse to cylinder axis ($R = 150\,\mu m$, r and L are irrelevant). Middle: diffusion along axis, with $L = 150\,\mu m$, and closed partitions ($r = 0$). Lower: diffusion along axis with partially open partitions ($L = 150\,\mu m$, $R = 150\,\mu m$, and $r = 105\,\mu m$). In all cases, the b value at which the signal has decayed by $1/e$ is quite close to the value from the straight line, so the $1/e$ value will yield a very close estimate of the average diffusivity.

negative. We note that the simulations presented in Fig. 3 are for $N = 100{,}000$ particles. The fractional statistical noise, $1/\sqrt{N}$, is about 0.3%; thus the decays in Fig. 3 taken out to 2.5 factors of e are relatively free of noise. This has been verified by repeating the same simulation several times, in selected cases, with virtually identical results.

The representative signal decays are displayed in Fig. 3: (upper) with the gradient transverse to the cylinder axis with $R = 150\,\mu m$ and (middle and lower) with a longitudinal gradient. This choice of cases avoids the

necessity of forming a powder average signal-decay, averaging over all cylinder (or gradient) orientations. The middle panel is for closed end caps ($L = 150\,\mu m$; $r = 0$ and R is irrelevant) and the bottom panel is for partly closed cells ($L = 150\,\mu m$, $R = 150\,\mu m$, $r = 105\,\mu m$, so the end caps are 49% open fraction of area). For each case, the decays were calculated at $t = 60$, 100, and 200 μs; the data selected to appear in Fig. 3 are at the time values showing the *largest* deviation from single exponential decay as a function of b.

Over the first factor of e in the decays shown in Fig. 3, the deviation from the straight line (simple exponential decay) is very small, less than 5%. Thus, less than a 5% error will occur if the NMR-determined diffusivity is taken as $1/b^*$, where b^* is the value of b for which the signal has decayed by $1/e$, instead of the negative of the slope of the straight line (the $b = 0$ limit). The largest deviations we have found in simulating many different geometries as in Fig. 1 are about 15%, though these occur with only a few sets of geometric parameters and time. We note that the deviations considered here are *systematic* errors. Measurement noise will result in random or statistical errors in determining D that may often be greater than the 5% systematic errors of Fig. 3.

Exact numerical results for the spin-echo (SE) decay have been reported for a one-dimensional system of uniformly spaced barriers ($L = 150\,\mu m$, in notation of Fig. 1), using a matrix-product technique [29]. Those results have been used here to derive a time-dependent diffusivity using Eq. (4), for values of bD_0 of 0.001, 0.1, 0.5, and 1.0. The $D_{(t)}^{SE}$ values yield values of S/V using Eq. (3b) with dimensionality $d = 1$; the results are presented in Fig. 4. This graph simultaneously reveals both

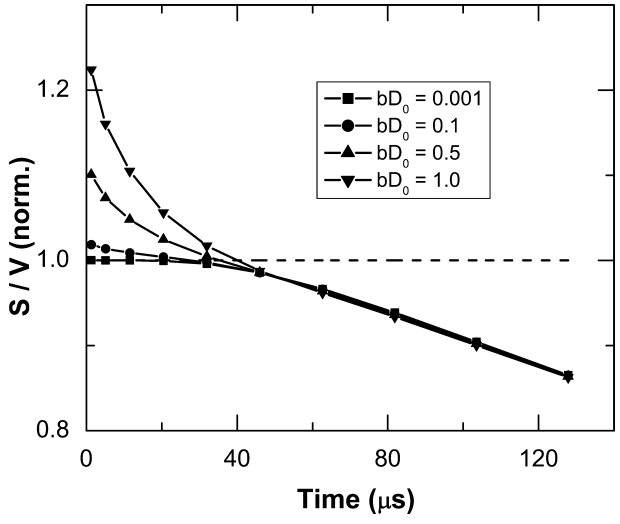

Fig. 4. Surface-to-volume S/V from NMR spin echoes (wide pulse or SE case) using Eq. (3b), normalized to the geometrical S/V. The system is a one-dimensional array of partitions spaced 150 μm. Exact numerical calculations of the echo amplitude attenuation were performed at several values of bD_0. Time-dependent diffusivity was calculated from Eq. (4).

effects: the inaccuracy in determining $D_{(t)}^{SE}$ outside the $b = 0$ limit and the error in S/V encountered by working outside the $t = 0$ limit. For short times and small bD_0, the S/V results are in excellent accord with the geometrical value of $2/L$.

At times of 40 μs and longer, there is essentially no dependence on the b value of the deduced S/V. Evidently, the echo amplitude decays here are very nearly single-exponential. As expected, with increasing time the S/V value decreases in qualitative accord with the results of the right side of Fig. 2. We note that these one-dimensional results cannot be compared directly to the three-dimensional results of Fig. 2. In addition, the $L = 150\,\mu m$ spacing of the partitions here leads to an approximately threefold decrease in the characteristic time scale, compared to Fig. 2, where the *diameter* is 300 μm (see Eq. (5)).

For times shorter than 40 μs, the S/V depends on the value of b, indicating that the echo amplitude decays are not single-exponential here. This non-exponential nature at short times has been analyzed in a recent work [12]. In the limit of zero time, this effect results in errors of 22% in S/V, using $bD_0 = 1$. It must be noted, however, that the large errors result from the high sensitivity of S/V to small changes in $D_{(t)}^{SE}$ in Eq. (3b) at short times where $D_{(t)}^{SE}$ and D_0 are nearly equal. In real experiments, this short-time region must be avoided anyway because S/V would be unduly sensitive to *random noise* in $D_{(t)}^{SE}$. For S/V values within ±15% of the actual geometrical S/V, with $bD_0 = 1$, times between 10 and 125 μs can be used.

5. Conclusions

Computer simulations of diffusive random-walks and numerical calculations have explored the time-dependent diffusion coefficient $D_{(t)}$ in restricted diffusion. The chosen geometries are periodic partitions in 1-D for the numerical work. The simulations modeled the interiors of cylinders with partially closed, periodically spaced partitions, a model of lung small-airways. The surface-to-volume ratios S/V determined from the simulations using the Mitra–Sen–Schwartz and de Swiet–Sen formulas (1) and (2), strictly valid only as time $t \to 0$, are compared to the exact values of the simulated geometries.

The first major result is that reasonably accurate S/V values (within ±15%) are obtained well outside the limit of time $t \to 0$. For closed vessels, the useful range extends to the remarkably small value of $D_{(t)}/D_0 = 0.25$; for fully or partially open vessels, the useful range is somewhat smaller. The errors encountered by working outside the $t \to 0$ limit can be reduced by use of the present results as a guide. Second, the NMR signals in restricted diffusion are not purely exponentially decaying

functions of the parameter b. Nevertheless, the difference between the diffusion values taken from the initial slope ($b \to 0$ limit which uniformly weights all spins) and the $1/e$ point of the decay (an experimentally practical scheme) remains small in all of our simulations. These results apply to both the narrow pulse and wide pulse experiments, the latter being equivalent to a static (dc) gradient in a spin-echo sequence, which makes minimal demands on the gradient hardware.

Thus, diffusion-NMR determinations of lung surface-to-volume ratios using inhaled gases appear to be quite feasible.

Acknowledgments

The authors gratefully acknowledge NIH support through Grant R01 HL70037 and support by AGA-Linde Healthcare through the Gas-Enabled Medical Innovation Fund. We appreciate the advice of D.A. Yablonskiy and his reading of the manuscript. The WU Department of Radiology has generously supported the authors' gas MRI efforts.

References

[1] D. Topgaard, C. Malmborg, O. Söderman, Restricted self-diffusion of water in a highly concentrated W/O emulsion studied using modulated gradient spin-echo NMR, J. Magn. Reson. 156 (2002) 195–201.
[2] D.G. Cory, A.N. Garroway, Measurement of translational displacement probabilities by NMR: an indicator of compartmentation, Magn. Reson. Med. 14 (1990) 435–444.
[3] P.P. Mitra, P.N. Sen, L.M. Schwartz, Short-time behavior of the diffusion coefficient as a geometrical probe of porous media, Phys. Rev. B 47 (1993) 8565–8574.
[4] P.P. Mitra, P.N. Sen, L.M. Schwartz, P. Le Doussal, Diffusion propagator as a probe of the structure of porous media, Phys. Rev. Lett. 68 (1992) 3555–3558.
[5] L.L. Latour, P.P. Mitra, R.L. Kleinberg, C.H. Sotak, Time-dependent diffusion coefficient of fluids in porous media as a probe of surface-to-volume ratio, J. Magn. Reson. 101 (1993) 342–346.
[6] T.M. de Swiet, P.N. Sen, Decay of nuclear magnetization by bounded diffusion in a constant field gradient, J. Chem. Phys. 100 (1994) 5597–5604.
[7] W.S. Price, Pulsed-field gradient NMR as a tool for studying translational diffusion: Part 1. Basic theory, Concepts Magn. Reson. 9 (1997) 299–336.
[8] E.O. Stejskal, J.E. Tanner, Spin diffusion measurements: spin echoes in the presence of a time-dependent gradient, J. Chem. Phys. 42 (1965) 288–292.
[9] H.C. Torrey, Nuclear spin relaxation by translational diffusion, Phys. Rev. 92 (1953) 962–969.
[10] E.O. Stejskal, Use of spin echoes in a pulsed magnetic-field gradient to study anisotropic, restricted diffusion and flow, J. Chem. Phys. 43 (1965) 3597–3603.
[11] P.P. Mitra, P.N. Sen, Effects of microgeometry and surface relaxation on NMR pulsed-field-gradient experiments: simple pore geometries, Phys. Rev. B 45 (1992) 143–156.
[12] A.L. Sukstanskii, J.J.H. Ackerman, D.A. Yablonskiy, Effects of barrier-induced nuclear spin magnetization inhomogeneities on diffusion-attenuated MR signal, Magn. Reson. Med. 50 (2003) 735–742.
[13] L.J. Zielinski, P.N. Sen, Effects of finite-width pulses in the pulsed-field gradient measurement of the diffusion coefficient in connected porous media, J. Magn. Reson. 165 (2003) 153–161.
[14] R.W. Mair, P.N. Sen, M.D. Hürlimann, S. Patz, D.G. Cory, R.L. Walsworth, The narrow pulse approximation and long length scale determination in xenon gas diffusion NMR studies of model porous media, J. Magn. Reson. 156 (2002) 202–212.
[15] R.W. Mair, G.P. Wong, D. Hoffmann, M.D. Hürlimann, S. Patz, L.M. Schwartz, R.L. Walsworth, Probing porous media with gas diffusion NMR, Phys. Rev. Lett. 83 (1999) 3324–3327.
[16] G.Q. Zhang, G.J. Hirasaki, CPMG relaxation by diffusion with constant magnetic field gradient in a restricted geometry: numerical simulation and application, J. Magn. Reson. 163 (2003) 81–91.
[17] M.D. Hurlimann, K.G. Helmer, T.M. de Swiet, P.N. Sen, C.H. Sotak, Spin echoes in a constant gradient and in the presence of simple restriction, J. Magn. Reson. 113 (1995) 260–264.
[18] J.B. West, Respiratory Physiology, Williams and Wilkins, Baltimore, 1990.
[19] E. Weibel, Design of airways and blood vessels considered as branching trees, in: R.G. Crystal, J.B. West, P.J. Barnes, E.R. Weibel (Eds.), The Lung: Scientific Foundation, Lippincott-Raven, Philadelphia, 1997, pp. 1061–1071.
[20] J.B. West, Pulmonary Pathophysiology, Williams and Wilkins, Baltimore, 1992.
[21] B.T. Saam, D.A. Yablonskiy, V.D. Kodibagkar, J.C. Leawoods, D.S. Gierada, J.D. Cooper, S.S. Lefrak, M.S. Conradi, MR imaging of diffusion of ^{3}He gas in healthy and diseased lungs, Magn. Reson. Med. 44 (2000) 174–179.
[22] M. Salerno, E.E. de Lange, T.A. Altes, J.D. Truwit, J.R. Brookeman, J.P. Mugler, Emphysema: hyperpolarized helium 3 diffusion MR imaging of the lungs compared with spirometric indexes-initial experience, Radiology 222 (2002) 252–260.
[23] D.A. Yablonskiy, A.L. Sukstanskii, J.C. Leawoods, D.S. Gierada, G.L. Bretthorst, S.S. Lefrak, J.D. Cooper, M.S. Conradi, Quantitative in vivo assessment of lung microstructure at the alveolar level with hyperpolarized ^{3}He diffusion MRI, Proc. Natl. Acad. Sci. USA 99 (2002) 3111–3116.
[24] M.W. Zemansky, R.H. Dittman, Heat and Thermodynamics, McGraw-Hill, New York, 1981, p. 256 and pp. 336–342.
[25] P.W. Bridgman, Dimensional Analysis, Yale University Press, New Haven, CT, 1931.
[26] C.P. Slichter, Principles of Magnetic Resonance, Springer, New York, 1996, pp. 597–601.
[27] L. van der Weerd, S.M. Melnikov, F.J. Vergeldt, E.G. Novikov, H. Van As, Modelling of self-diffusion and relaxation time NMR in multicompartment systems with cylindrical geometry, J. Magn. Reson. 156 (2002) 213–221.
[28] P.T. Callaghan, Principles of Nuclear Magnetic Resonance Microscopy, Clarendon Press, Oxford, 1991, p. 349.
[29] A.L. Sukstanskii, D.A. Yablonskiy, Effects of restricted diffusion on MR signal formation, J. Magn. Reson. 157 (2002) 92–105.